https://doi.org/10.5194/egusphere-2026-5054
Preprint. Discussion started: 31 August 2026


# Evaluation of EarthCARE retrievals of ice microphysics and vertical wind using in-situ aircraft observations

Robin J. Hogan[1], Bernat Puigdomènech Treserras[2], Shannon L. Mason[1], Alexei Korolev[3], Zhipeng Qu[3], Kamil Mroz[1], David P. Donovan[4], Pavlos Kollias[5,2], and Mark D. Fielding[1]

[1]European Centre for Medium-Range Weather Forecasts, Reading, UK
[2]Department of Atmospheric and Oceanic Sciences, McGill University, Montreal, Quebec, Canada
[3]Atmospheric Science and Technology Directorate, Environment and Climate Change Canada, Toronto, Ontario, Canada
[4]Royal Netherlands Meteorological Institute (KNMI), de Bilt, the Netherlands
[5]Division of Atmospheric Science, Stony Brook University, Stony Brook, NY, USA

**Correspondence:** Robin J. Hogan (robin.hogan@ecmwf.int)

**Abstract.** The novel observational capabilities of the EarthCARE satellite promise the most accurate retrievals of the vertical profile of ice clouds yet achieved from space, but independent evaluation is essential. In this paper we use in-situ sampling from five underflights of EarthCARE in ice clouds between $-10$ and $-45$°C during the UK "VERIFY" and Canadian "ECALOT" campaigns to evaluate and improve its microphysical and vertical-wind retrievals, as well as testing prior assumptions such as the mass–size relationship and the radar ice scattering model. We find that, to a good approximation, the small-scale fluctuations in radar-measured Doppler velocity can be attributed to vertical wind and the larger-scale averages to ice terminal fall speed. When EarthCARE's "C-CD" algorithm is updated to exploit this finding, its vertical wind retrieval is able to capture the amplitude and phase of gravity waves measured by the aircraft. Retrievals of IWC and extinction by the radar-only "C-CLD" algorithm, the lidar-only "A-EBD" algorithm and the synergistic "ACM-CAP" algorithm, are in good agreement with the aircraft but highlight the important challenge of retrieving ice particle density. Comparing the 94-GHz radar reflectivity observed by EarthCARE with values computed from the aircraft probes enables us to successfully validate the Self-Similar Rayleigh-Gans scattering model even when non-Rayleigh scattering reduces the reflectivity below the equivalent Rayleigh value by 15 dB. However, the calculations of reflectivity-weighted terminal fall speed from the aircraft are systematically 15–30% higher than measured by EarthCARE's Doppler radar, suggesting the need for further work on models of ice fall speed.

## 1 Introduction

Launched in May 2024, the EarthCARE satellite (Illingworth et al., 2015) is providing new insights into the properties of clouds and aerosols. Its Cloud Profiling Radar (CPR) is the first spaceborne radar that can use the Doppler shift of the backscattered signals to infer the vertical velocity of cloud and precipitation particles. The operational CPR "Corrected Doppler" (C-CD) algorithm (Kollias et al., 2023) attempts to separate the measured Doppler velocity into the contribution from vertical wind, which can drive microphysical processes within the cloud (e.g. Hogan et al., 2002; Atlas and Bretherton, 2023), and terminal fall velocity, which is a key uncertainty in weather and climate models (Jakob, 2002). EarthCARE's Atmospheric Lidar

https://doi.org/10.5194/egusphere-2026-5054
Preprint. Discussion started: 31 August 2026


**Table 1.** Summary of research flights used in this paper. Density factor is defined in section 2.3.

| Date | Flight | EarthCARE frame | Aircraft temperature | Typical radar reflectivity, $Z$ | Density factor, $f_\rho$ | Cloud type, comments |
|---|---|---|---|---|---|---|
| 14 Jan 2025 | VERIFY6 | 03589D | $-45°$C | $-30$ dBZ | 0 | Thin cirrus, no Doppler |
| 7 Nov 2024 | VERIFY2 | 02531D | $-45°$C | $-15$ dBZ | 0 | Cirrus, gravity wave |
| 4 Nov 2024 | ECALOT3 | 02487D | $-17°$C | 0 dBZ | 0 | Nimbostratus |
| 27 Jan 2025 | ECALOT6 | 03794D | $-23°$C | 0 dBZ | 0.1 | Nimbostratus, gravity wave |
| 18 Nov 2024 | VERIFY4 | 02702D | $-10°$C | 10 dBZ | 0.1 | Nimbostratus, non-Rayleigh scattering |

(ATLID) is a high spectral resolution lidar (HSRL), enabling it to measure the backscatter by air molecules within a cloud. The operational ATLID "Extinction, Backscatter and Depolarization" (A-EBD) algorithm (Donovan et al., 2024) uses this signal to infer the vertical profile of cloud extinction coefficient, the most important property for determining a cloud's interaction with atmospheric radiation. Synergy retrievals are provided by the "ACM-CAP" algorithm (Mason et al., 2023), which combines ATLID, CPR and the Multi-Spectral Imager (MSI) to obtain the microphysical properties of Clouds, Aerosols and Precipitation.

Naturally, it is important to evaluate new products against in-situ measurements from aircraft; while not perfect, in-situ measurements are the closest we can get to "truth". In this paper we use data from the UK Facility for Airborne Atmospheric Measurements (FAAM) taken during the "VERIFY" campaign, and from the Canadian Convair-580 research aircraft during "ECALOT" (EarthCARE Commissioning Cal/Val Campaign in Ottawa), with a focus on ice clouds. The five suitable flights are listed in Table 1 in order of increasing observed radar reflectivity at the level of the aircraft. Flights in which the aircraft sampled significant amounts of supercooled water were excluded: the added difficulty for the retrievals in such conditions makes the topic of evaluating EarthCARE in mixed-phase clouds best served by its own paper. In addition to comparing meteorological quantities such as IWC and vertical wind speed, we also compare 94-GHz radar reflectivity factor, $Z_{94}$, computed from the aircraft size distributions to the CPR observations. Since $Z_{94}$ is sensitive to the assumed mass–size distribution and the treatment of non-Rayleigh scattering by larger particles, this provides an evaluation of both the scattering assumptions made within the ACM-CAP retrieval algorithm, and also the cloud-radar forward models used for model evaluation and data assimilation (e.g. Fielding and Janisková, 2020).

Section 2 describes the aircraft platforms, instrumentation, and how the various quantities were computed from the measured size distribution. Section 3 summarizes the three EarthCARE retrieval algorithms evaluated in the paper and describes the changes that have been made after launch in the light of evaluation data such as presented in this paper. Then in section 4 the results from the five flights are presented including a detailed discussion of the implications for each of the retrieved variables.

https://doi.org/10.5194/egusphere-2026-5054
Preprint. Discussion started: 31 August 2026


## 2 Description of aircraft platforms and processing

### 2.1 Facility for Atmospheric Airborne Measurements (FAAM)

The FAAM underflights of EarthCARE used in this paper are from the VERIFY campaign that took place to the north-west of the UK: VERIFY4 over Northern Ireland and VERIFY2 and VERIFY6 over the sea off the coast of Scotland. FAAM was a BAe-146 aircraft owned and operated by the UK Natural Environment Research Council, carrying a comprehensive suite of cloud physics probes (Cotton et al., 2013). Two optical array probes (OAPs) are combined to derive the particle size distribution (PSD): the DMT CIP-15 (Droplet Measurement Technologies Cloud Imaging Probe with 15-$\mu$m resolution) measures particles of size 15–960 $\mu$m while the CIP-100 measures particles of size 100-6400 $\mu$m. Particle sizes up to 600 $\mu$m were taken from CIP-15 and larger particles from CIP-100. Particles are binned in terms $D$, the mean of the particle dimensions measured parallel and perpendicular to the photodiode array; note that this is around 80% of the "maximum dimension" that is sometimes used for binning ice PSDs (Hogan et al., 2012).

Bulk IWC is provided by a deep-cone Nevzorov probe; by excluding cases with supercooled liquid water present at flight level, we simply use the measurement by the total water probe as IWC. The vertical velocity of the air is provided by the aircraft's GPS-corrected inertial navigation system combined with a pressure sensor in the nose cone.

### 2.2 NRC Convair-580 Research Aircraft

The ECALOT campaign involved flights of the National Research Council (NRC) of Canada's Convair-580 research aircraft, in the vicinity of Ottawa, Canada. Again, two OAPs are combined to form a composite PSD: the SPEC 2D-S (Stratton Park Engineering Company 2D-Stereo probe) with 10-$\mu$m resolution in the nominal size range 10–1280 $\mu$m, and the SPEC High Volume Precipitation Spectrometer (HVPS) with 0.15 mm resolution in the nominal size range 0.15–19.2 mm. Composite PSDs were composed of 2D-S particles of size 100–980 $\mu$m and HVPS particles of size 1.05–38.4 mm. Particles are binned in terms of their dimension in the direction perpendicular to the flight direction, which is assumed to be statistically equivalent to the mean dimension $D$ used by FAAM, on average. The image processing included the retrieval of both completely and partially viewed images, enabling the extension of PSDs to larger sizes. Sizes smaller than 100 $\mu$m were not reported due to contamination by diffraction artifacts and uncertainties in the sample volume, but the two ECALOT cases considered in this paper were dominated by particles larger than this size. Ice-shattering artifacts were filtered out using an anti-shattering algorithm. The thermodynamic state of clouds was identified based on complementary measurements from the Rosemount Icing Detector (RICE) and the forward-scattering DMT Cloud Droplet Probe (CDP) and SPEC Fast Cloud Droplet Probe (FCDP). Thus, if the RICE output frequency did not decrease and the total particle concentration measured by CDP and FCDP remained below 5 cm$^{-3}$, the cloud was identified as pure ice. The Convair-580 also carries a Nevzorov probe, and the processed data include both IWC and liquid water content. During processing, the Nevzorov IWC data have been scaled up by up to around 50% to account for the ice particle rebound out of the total-water-concent sensor. However, since this scaling has not been performed on FAAM data, the figures in section 4 show the unscaled IWC values for both VERIFY and ECALOT

https://doi.org/10.5194/egusphere-2026-5054
Preprint. Discussion started: 31 August 2026


flights, but with a grey band extending upwards to indicate the uncertainty due to possible rebounding. Vertical wind is derived from a five-hole Rosemount-858AJ probe (Williams et al., 2000).

### 2.3 Calculation of ice microphysical and scattering properties from the PSD

The OAPs provides PSDs that we denote as $n(D)$ such that $n(D)dD$ is the number concentration of particles in the size range $D$ to $D+dD$. Ice water content is then given by

$$\mathrm{IWC} = \int_0^\infty n(D)m(D)dD, \tag{1}$$

where $m(D)$ is the mass of particles of mean dimension $D$. Our default choice is the Brown and Francis (1995) relationship (hereafter BF95), which is used as the a-priori assumption in ACM-CAP, and which Hogan et al. (2006) found to lead to good agreement between measured radar reflectivity factor and values calculated by aircraft. In SI units it is expressed as (Hogan et al., 2012)

$$\begin{aligned} m(D) &= 480D^3; && D < 97\times10^{-6}\ \mathrm{m}, \\ m(D) &= 0.0185D^{1.9}; && D \geq 97\times10^{-6}\ \mathrm{m}, \end{aligned} \tag{2}$$

where the first row ensures the density of small ice particles does not exceed that of solid ice. Two of the flights in this paper showed evidence of denser particles than BF95 being present. Mason et al. (2018) showed that the variability in observed mass–size relationships (such as due to riming) could be well captured by single "density factor" $f_\rho$ varying between 0 for the low-density aggregates represented by BF95 and 1 for solid ice spheres. To represent the denser cases we consider also the mass–size relationship for $f_\rho = 0.1$, which in SI units is

$$\begin{aligned} m(D) &= 480D^3; && D < 97\times10^{-6}\ \mathrm{m}, \\ m(D) &= 0.051D^{2.01}; && D \geq 97\times10^{-6}\ \mathrm{m}. \end{aligned} \tag{3}$$

Extinction coefficient in the geometric optics approximation is given by

$$\alpha = 2\int_0^\infty n(D)A(D)dD, \tag{4}$$

where $A(D)$ is the projected particle area. Since PSDs were not provided binned by area, we use the relationship of Francis et al. (1998) derived from aircraft data:

$$\begin{aligned} A(D) &= \pi(D/2)^2; && D < 126\times10^{-6}\ \mathrm{m}, \\ A(D) &= 0.02683D^{1.624}; && D \geq 126\times10^{-6}\ \mathrm{m}, \end{aligned} \tag{5}$$

where the first row prevents the projected area exceeding that of a circle of diameter $D$.

Two measures of particle size are compared between aircraft and satellite: effective radius defined as (e.g. Francis et al., 1998)

$$r_e = \frac{3\mathrm{IWC}}{2\rho_i\alpha}, \tag{6}$$

https://doi.org/10.5194/egusphere-2026-5054
Preprint. Discussion started: 31 August 2026


where $\rho_i$ is the density of solid ice, and the ratio of the third and second moments of the distribution $D_m = M_3/M_2$ (Field et al., 2005), where

$$M_k = \int_0^\infty n(D) D^k dD. \tag{7}$$

Note that $r_e$ and $D_m$ can be different by more than an order of magnitude when large particles are present, because $r_e$ is dependent on the mass–size and area-size relationships while $D_m$ is not.

The effective 94-GHz radar reflectivity factor in ice clouds may be written as (e.g. Hogan et al., 2006)

$$Z_{94} = \frac{|K_i|^2}{|K_{\mathrm{ref}}|^2} \left(\frac{6}{\pi \rho_i}\right)^2 \int_0^\infty n(D) m(D)^2 \eta(D) dD, \tag{8}$$

where $|K_i|$ is the dielectric factor of solid ice (0.174 at all radar frequencies), $|K_{\mathrm{ref}}| = 0.75$ is the reference dielectric factor for the 94-GHz calibration convention of EarthCARE, and $\eta(D)$ expresses the deviation of the backscatter from Rayleigh scattering, relevant when the size of a particle approaches or exceeds the wavelength. As in ACM-CAP, we use the Self-Similar Rayleigh-Gans Approximation (SSRGA) of Hogan and Westbrook (2014) to compute $\eta(D)$. The SSRGA parameters appropriate for "Westbrook aggregates" reported by Hogan et al. (2017) are used ($\alpha_{\mathrm{eff}} = 0.83$, $\kappa = 0.09$, $\beta = 0.55$, $\gamma = 2.0$ and $\zeta_1 = 0.28$), but we have found the best result by assuming that the aspect ratio of the monomer crystals that compose the aggregate is 1, which removes the modest backscatter enhancement described by Hogan et al. (2017). It can be seen in (8) that $Z_{94}$ is a sensitive function of particle mass, and as reported by Hogan et al. (2006), a factor-of-two change in the mass–size relationship results in a 6 dB change to computed radar reflectivity. For most of the cases in this paper the particles are small enough that Rayleigh scattering applies (i.e. $\eta \simeq 1$), but in one of the cases the non-Rayleigh correction provided by SSRGA is very large, so we plot both $Z_{94}$ and the Rayleigh equivalent obtained by setting $\eta = 1$.

Finally, the Doppler velocity is computed as the sum of the vertical wind ($w$) and the reflectivity-weighted terminal velocity ($v_T$): $v_D = w + v_T$, where

$$v_T = \left(\frac{\rho_{\mathrm{ref}}}{\rho}\right)^{1/2} \int_0^\infty n(D) m(D)^2 \eta(D) v(D, \rho_{\mathrm{ref}}) dD \Big/ \int_0^\infty n(D) m(D)^2 \eta(D) dD. \tag{9}$$

Here $v(D, \rho_{\mathrm{ref}})$ is the terminal velocity of an individual particle at a reference air density of $\rho_{\mathrm{ref}} = 0.5$ kg m$^{-3}$, and $\rho$ is the actual air density at the altitude of the aircraft. We use the Heymsfield and Westbrook (2010) model for $v(D, \rho)$, which is dependent on the particle mass and the area ratio (i.e. the ratio of the actual projected area $A(D)$ to the area of a circle of diameter $D$). We follow the EarthCARE convention that $v_D$ is positive when in a downward direction, and since an important question addressed in this paper is how to partition it into $w$ and $v_T$, we adopt the same positive-down convention for all velocities including vertical wind.

https://doi.org/10.5194/egusphere-2026-5054
Preprint. Discussion started: 31 August 2026


## 3 Retrieval algorithms

### 3.1 CPR Corrected Doppler (C-CD)

The operational C-CD algorithm (Kollias et al., 2023) performs numerous corrections to the raw measured Doppler velocity to make it useful for meteorological research, including correction for antenna mispointing (Puigdomènech Treserras et al., 2025), correction for non-uniform beam filling effects, some horizontal averaging to reduce uncertainty and a velocity dealiasing correction. After these steps, the corrected Doppler velocity, $v_D$, is used to estimate the reflectivity-weighted hydrometeor terminal fall speed, $v_T$ (Puigdomènech Treserras et al., 2026). This retrieval technique assumes that microphysical and thermodynamic conditions are approximately stationary within a local neighborhood around each target. Under this assumption, and when the analysis is restricted to a narrow range of reflectivity, $Z_{94}$, and temperature, $T$, the expected variability of $v_T$ is small compared with the variability introduced by vertical air motion and measurement noise. Using this assumption, the retrieval selects an optimal adaptive averaging scale by balancing measurement uncertainty against geophysical variability, providing a robust estimate of $v_T$.

At the time of launch, the $v_T$ retrieval used a simplified neighbourhood-averaging approach (following the general idea of Protat and Williams, 2011). The $v_D$ samples were grouped into 3-dBZ bins over a set of along-track averaging windows with lengths of 10–40 km, combined with a small vertical window (three range bins) centered on the target gate. To preserve spatial representativeness while maximizing sample size, the method attempted the calculation across the sequence of window lengths and retained the most local estimate available. However, the initial comparison to aircraft data in this study revealed that structure in the vertical wind field was being incorrectly interpreted as variations in terminal fall speed. A more exhaustive analysis determined that the algorithm reported estimates whose uncertainty exceeded the geophysical variability within the averaging window. Therefore, the comparisons in this paper use the novel approach described in Puigdomènech Treserras et al. (2026) that will be operational from the BD baseline version of the EarthCARE C-CD data. In the updated technique, the candidate along-track averaging scales are extended up to ∼250 km, allowing the retrieval to select the scale that minimizes within-window geophysical variability under the local-stationarity assumption, rather than being constrained to short (10–40 km) windows that can result in higher uncertainty.

### 3.2 CPR Cloud and Precipitation Microphysics (C-CLD)

The C-CLD algorithm (Mroz et al., 2023) is based on a variational (also known as optimal estimation) framework to retrieve hydrometeor characteristic-size and water content by combining $Z_{94}$, $v_T$ and (if available) the path-integrated attenuation (PIA; Sasikumar et al., 2025). The algorithm is composed of dedicated sub-algorithms, with a different one applied to the radar measurements depending on the type of cloud or precipitation observed: liquid cloud and light drizzle, ice/snow, ice/snow associated with cold rain and warm rain. In the original implementation, uncertainties in ice particle mass–size relationships were handled with an ensemble approach, that is, the retrieval was performed for several prescribed density (riming) assumptions. The solution yielding the minimum cost function was then retained as the final estimate. However, this approach led to strong along-track variability, because the characteristics of the CPR $v_T$ characteristics were unknown at the time of implementa-

https://doi.org/10.5194/egusphere-2026-5054
Preprint. Discussion started: 31 August 2026


tion and the a-priori information was not well balanced by the observations. In addition, the Doppler velocity forward model, which maps the microphysical parameters into radar measurement space, sometimes introduced inconsistencies between the observations and the a-priori information. To mitigate these issues, both the a-priori constraints and the forward-model relationships have been refined using post-launch observations, better constraining the solution space and stabilizing the retrieval. The ensemble approach is also treated differently and the mass–density assumptions are no longer defined on a per-profile basis but are harmonized along-track. For ice clouds with very small particles, the ensemble-mean solution is used, because the uncertainty in the Doppler-velocity measurements exceeds the differences in forward-modelled Doppler velocity among ensemble members. These improvements lead to more homogeneous results.

### 3.3 ATLID Extinction, Backscatter and Depolarization (A-EBD)

A-EBD uses a variational algorithm to derive the vertical profile of extinction coefficient from the measured "Mie" (i.e. particulate) and Rayleigh channels of EarthCARE's HSRL (Donovan et al., 2024). A-EBD delivers extinction, lidar-ratio and depolarization-ratio profiles for both aerosols (at different horizontal resolutions) and clouds (at a 1-km horizontal scale). The A-EBD algorithm is run as part of a larger processor that first runs a more conventional HSRL aerosol retrieval (A-AER) and a target classification procedure (A-TC, Irbah et al., 2023). Together, A-AER and A-TC help supply the prior assumptions for A-EBD. For the "BA" data product baseline used in this paper, bug fixes and other modest improvements have been made mainly in the A-TC procedure compared to the pre-launch algorithm described by Irbah et al. (2023), but these were in areas such as aerosol–cloud discrimination and are not relevant to the cases presented in the present study. The A-EBD algorithm has not changed significantly since the pre-launch description provided by Donovan et al. (2024).

### 3.4 ATLID-CPR-MSI Cloud, Aerosol and Precipitation (ACM-CAP)

The operational ACM-CAP algorithm combines observations from EarthCARE's radar, lidar and imager and uses a variational approach to simultaneously retrieve profiles of the microphysical properties of liquid clouds, ice clouds, precipitation and aerosol (Mason et al., 2023). Ice clouds are described by three independent variables: geometric extinction coefficient $\alpha$, normalized number concentration $N_0^* = M_2^4/M_3^3$ (where moment $M_k$ is given by Eq. 7) and density factor $f_\rho$. From these, all other microphysical variables can be calculated, such as IWC and $r_e$. The variational approach finds the combination of these variables that best matches $Z_{94}$, $v_T$ (from C-CD), lidar "Mie" and "Rayleigh" backscatters, and the solar and infrared radiances, while tending back towards a-priori values when some observational information is missing, for example deep in an ice cloud where the lidar has been fully attenuated. During the EarthCARE commissioning phase it was necessary to check and in some cases adjust the values and uncertainties of the a-priori assumptions, as is now described.

Mason et al. (2018) originally described the retrieval of a density factor $f_\rho$ from multiple vertically-pointing Doppler radars, based on the fact that denser particles fall faster. A prior value of $f_\rho = 0$ ensures that by default the ice density tends towards that of unrimed aggregates. At the time of launch it was unclear how reliable the Doppler velocity would be and how easy it would be to extract the terminal velocity component $v_T$, so a reasonably large uncertainty was applied to it, but with a low uncertainty on the prior value of $f_\rho$ to ensure the retrieved density factor did not deviate far from zero. The aircraft data in this

https://doi.org/10.5194/egusphere-2026-5054
Preprint. Discussion started: 31 August 2026


paper suggest that three of the cases have $f_\rho \simeq 0$ and two have $f_\rho \simeq 0.1$, but ACM-CAP has little skill in retrieving it, partly due to inaccuracies in forward modelling $v_T$, as described in section 4.2. Therefore, the main ACM-CAP retrieval assumes a fixed value of $f_\rho = 0$, but in the final two cases we also consider alternative retrievals assuming a fixed value of $f_\rho = 0.1$ in order to investigate how whether the retrieved microphysical properties would be improved if $f_\rho$ could be correctly retrieved. In section 4.5 we discuss the extent to which it may be possible to retrieve $f_\rho$ rather than having it tightly constrained by prior assumptions.

To ensure the retrieval of $\alpha$ and $N_0^*$ is reasonable when only one of the radar or lidar detects the cloud, ACM-CAP follows Delanoe et al. (2008) and uses a state variable $N_0' = N_0^*/\alpha^{0.6}$ with a temperature-dependent (but IWC-independent) prior estimate. However, in ice clouds detected by both EarthCARE's radar and its lidar, it has been found that the retrieved $N_0'$ is higher than the values proposed by Delanoe et al. (2008), most likely because they were derived from aircraft PSDs in which particles smaller than 100 $\mu$m were neglected. We have therefore revised the prior $N_0'$ such that $\ln N_0'$ varies linearly with temperature from $N_0' = 1.0 \times 10^7$ m$^{-3.4}$ at 0°C to $N_0' = 1.5 \times 10^{11}$ m$^{-3.4}$ at $-55$°C, but is capped to these values outside this temperature range. This finding has implications for the way that ice clouds are parameterized in models, but this will be explored in a future paper.

A final relevant change to ACM-CAP since launch arose from the finding that it tended to retrieve higher extinction that A-EBD, even though information on extinction is primarily derived from the same high spectral resolution lidar. This was traced to the different values of "equivalent-area radius", $r_A$, used in the treatment of lidar multiple scattering. The strength of lidar multiple scattering on the measured signal in ice clouds depends on the width of the narrow forward lobe in the scattering phase function, which is inversely proportional to the physical radius of the particle. The question is how to find the appropriate radius to use for a distribution of particles. Originally, ACM-CAP used the definition of Hogan (2006), which is derived to compute the correct mean-squared angular width of the forward lobe. Unfortunately, this over-weights the small particles in the distribution with the widest forward lobes. We have found that a much better fit is obtained with the definition

$$r_A = \int_0^\infty n(D)A(D)\left[\frac{A(D)}{\pi}\right]^{1/2} dD \Big/ \int_0^\infty n(D)A(D)dD. \qquad (10)$$

Here, $(A/\pi)^{1/2}$ is simply the radius of a circle with the same cross sectional area as an individual particle of cross-sectional area $A$, and hence $r_A$ is the $A$-weighted average of this quantity over the size distribution. This weighting is appropriate since the scattering cross-section in the geometric-optics approximation is proportional to $A$. A future paper will explore further the effect of different values of $r_A$ in modelling multiple scattering.

## 4 Results

Table 1 lists the five ECALOT and VERIFY flights used in this paper in order of increasing radar reflectivity at the altitude of the aircraft. The comparisons are plotted in Figs. 1–10, where the first figure from each case compares the radar quantities and the second compares the microphysical retrievals. The raw aircraft measurements are reported at a scale of around 100 m, but to reduce sampling noise a 500-m moving average has been applied, except for Doppler velocity and vertical wind where it is

https://doi.org/10.5194/egusphere-2026-5054
Preprint. Discussion started: 31 August 2026


**Table 2.** Summary of the comparison of aircraft and EarthCARE data for each of the five underflights. Two numbers are provided for each flight and quantity being compared. The first indicates the median of the values derived from aircraft Optical Array Probes; all variables except $\alpha$ and $D_m$ are dependent on the assumed density factor, $f_\rho$, which was chosen to give the best match in IWC with the Nevzorov probe and is shown at the top of each column. The second number gives the difference in the medians (EarthCARE minus aircraft). Only samples corresponding to a simultaneous in-cloud measurement by the aircraft and EarthCARE within 30 km of the point of closest interception are considered (i.e. closer than around 0.25° in latitude to the vertical dashed lines in Figs. 1–10). The small differences in aircraft-measured extinction ($\alpha$) for the A-EBD and ACM-CAP rows are due to the differences in cloud detection between these two algorithms. The default ACM-CAP retrieval assumes a density factor of $f_\rho = 0$ and so is denoted 'ACM-CAP (0)', but for ECALOT6 and VERIFY4 where the Nevzorov probe suggests a value of 0.1 is appropriate, the retrieval has been re-run and is shown as "ACM-CAP (0.1)". Some retrievals are not available due to either the radar signal being too low for EarthCARE to make a Doppler measurement, or to the cloud being too thick for EarthCARE's lidar to penetrate to the altitude of the aircraft.

| Variable | Product | VERIFY6 | | VERIFY2 | | ECALOT3 | | ECALOT6 | | VERIFY4 | |
|---|---|---|---|---|---|---|---|---|---|---|---|
| | | $f_\rho = 0$ | | $f_\rho = 0$ | | $f_\rho = 0$ | | $f_\rho = 0.1$ | | $f_\rho = 0.1$ | |
| $Z$ (dBZ) | C-FMR | −29.0 | −0.2 | −13.0 | −2.5 | 1.2 | −0.5 | 1.1 | +0.0 | 10.3 | −0.2 |
| $v_T$ (m s$^{-1}$) | C-CD | Not available | | 0.51 | −0.07 | 1.19 | −0.20 | 0.99 | −0.13 | 1.30 | −0.38 |
| IWC (g m$^{-3}$) | C-CLD | Not available | | 0.0256 | −28% | 0.0468 | −33% | 0.0797 | −7% | 0.28 | +33% |
| | ACM-CAP (0) | 0.0028 | −28% | 0.0256 | +15% | 0.0468 | +9% | 0.0797 | +26% | 0.28 | +53% |
| | ACM-CAP (0.1) | | | | | | | | +13% | | +14% |
| $\alpha$ (km$^{-1}$) | A-EBD | 0.142 | +7% | 0.794 | +40% | 0.914 | +40% | Not available | | Not available | |
| | ACM-CAP (0) | 0.142 | −15% | 0.784 | +52% | 0.948 | +23% | 1.53 | +70% | 3.34 | +151% |
| | ACM-CAP (0.1) | | | | | | | | +33% | | +54% |
| $r_e$ ($\mu$m) | ACM-CAP (0) | 34.1 | −22% | 52.5 | −24% | 84.0 | −14% | 84.6 | −24% | 140.7 | −40% |
| | ACM-CAP (0.1) | | | | | | | | −11% | | −25% |
| $D_m$ ($\mu$m) | ACM-CAP (0) | 70 | −19% | 196 | −41% | 1088 | −22% | 574 | −2% | 2251 | −35% |
| | ACM-CAP (0.1) | | | | | | | | −14% | | −48% |

interesting to see the presence of small-scale turbulence, even if it is at too fine a scale to be detected by EarthCARE. Table 2 summarises the comparison of key variables defined in section 2.3, where for each flight and variable we show the median of the aircraft values within 30 km of the point of closest interception, followed by the difference between the EarthCARE and aircraft median. The median is used rather than the mean to suppress the effect of outliers, including spikes caused by EarthCARE detecting the aircraft.

As explained in section 2.3, computing mass-sensitive ice-cloud properties from OAPs requires an assumption about the mass–size relationship, which we select to provide the best match in IWC between the OAPs and the Nevzorov probe. The first three cases are best fitted by a density factor of $f_\rho = 0$ (i.e. the BF95 relationship), as shown by comparing the red and grey lines in Figs. 2f, 4f and 6f, while the last two cases are best fitted by the denser $f_\rho = 0.1$ relationship given by (3), as demonstrated in Figs. 8f and 10f. As discussed in section 3.4, ACM-CAP cannot yet confidently retrieve $f_\rho$, so the default

https://doi.org/10.5194/egusphere-2026-5054
Preprint. Discussion started: 31 August 2026


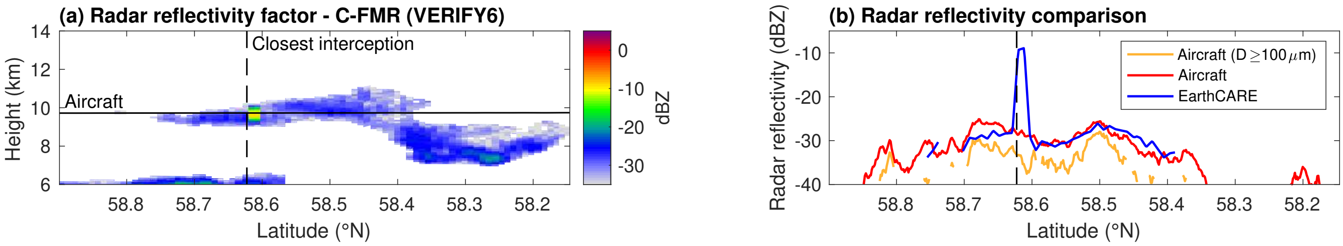


**Figure 1.** (a) EarthCARE 94-GHz radar reflectivity factor from the C-FMR product for frame 03589D on 14 January 2025, and (b) comparison with reflectivity calculated from the ice particle size distribution measured by the FAAM aircraft during the VERIFY6 flight assuming the BF95 mass–size distribution. The aircraft is seen clearly by EarthCARE as a spike in reflectivity. Since the reflectivity was so low, no reliable Doppler velocity measurements were available in this case. Note that in this and subsequent figures, latitude is shown decreasing from left to right to conform to the convention that EarthCARE data are displayed with sample time increasing from left to right.

version assumes a fixed $f_\rho = 0$, but in the last two cases an alternative retrieval is performed with a fixed $f_\rho = 0.1$; this is also shown in Table 2, and is depicted by dashed blue lines in Figs. 8 and 10.

In the following four subsections we evaluate the various EarthCARE retrievals, in each case considering the evidence from all the flights available.

### 4.1 94-GHz radar reflectivity factor

We first compare $Z_{94}$ between the EarthCARE radar measurement and the value calculated from the aircraft OAPs. As explained by Hogan et al. (2006), in the Rayleigh scattering regime this is a very sensitive test of the mass–size relationship since a factor-of-two error in the particle masses used in analysing the OAP data leads to a 6-dB difference in radar reflectivity. Radar reflectivity assuming Rayleigh scattering, $Z_{\mathrm{Ray}}$, has also been computed from the OAPs in each flight. In the first flight the particles were small and $Z_{94}$ is indistinguishable from $Z_{\mathrm{Ray}}$. Figure 1b shows excellent agreement between the aircraft and EarthCARE radar (except where the radar detects the aircraft), with a difference in medians of only 0.2 dB (Table 2). Also shown in orange is the reflectivity calculated from the aircraft OAPs but neglecting particles smaller than 100 $\mu$m; the difference of up to 10 dB indicates that up to 90% of the reflectivity is due to these small particles. This suggests that it may be necessary to reassess the findings of Field et al. (2005) and Delanoe et al. (2008) who both neglected these small particles in their characterization of ice size distributions using aircraft data. Note that in all other cases in this paper, particles smaller than 100 $\mu$m contributed very little to the bulk microphysical properties.

The ECALOT3 and ECALOT6 flights sampled somewhat larger particles ($D_m$ in the range 0.5–1 mm) leading to $Z_{\mathrm{Ray}}$ being slightly (and intermittently) larger than $Z_{94}$, as shown by the pink lines in Figs. 5b and 7b, but again the agreement with $Z_{94}$ is very good. The one case with poor agreement is VERIFY2 (Fig. 3b), in which we find the aircraft $Z_{94}$ (which is virtually identical to $Z_{\mathrm{Ray}}$) to be around 3 dB more than the EarthCARE measurement. This is difficult to explain in terms of the mass–size relationship: we would need to decrease the mass significantly *below* that of BF95 which would lead to much

https://doi.org/10.5194/egusphere-2026-5054
Preprint. Discussion started: 31 August 2026


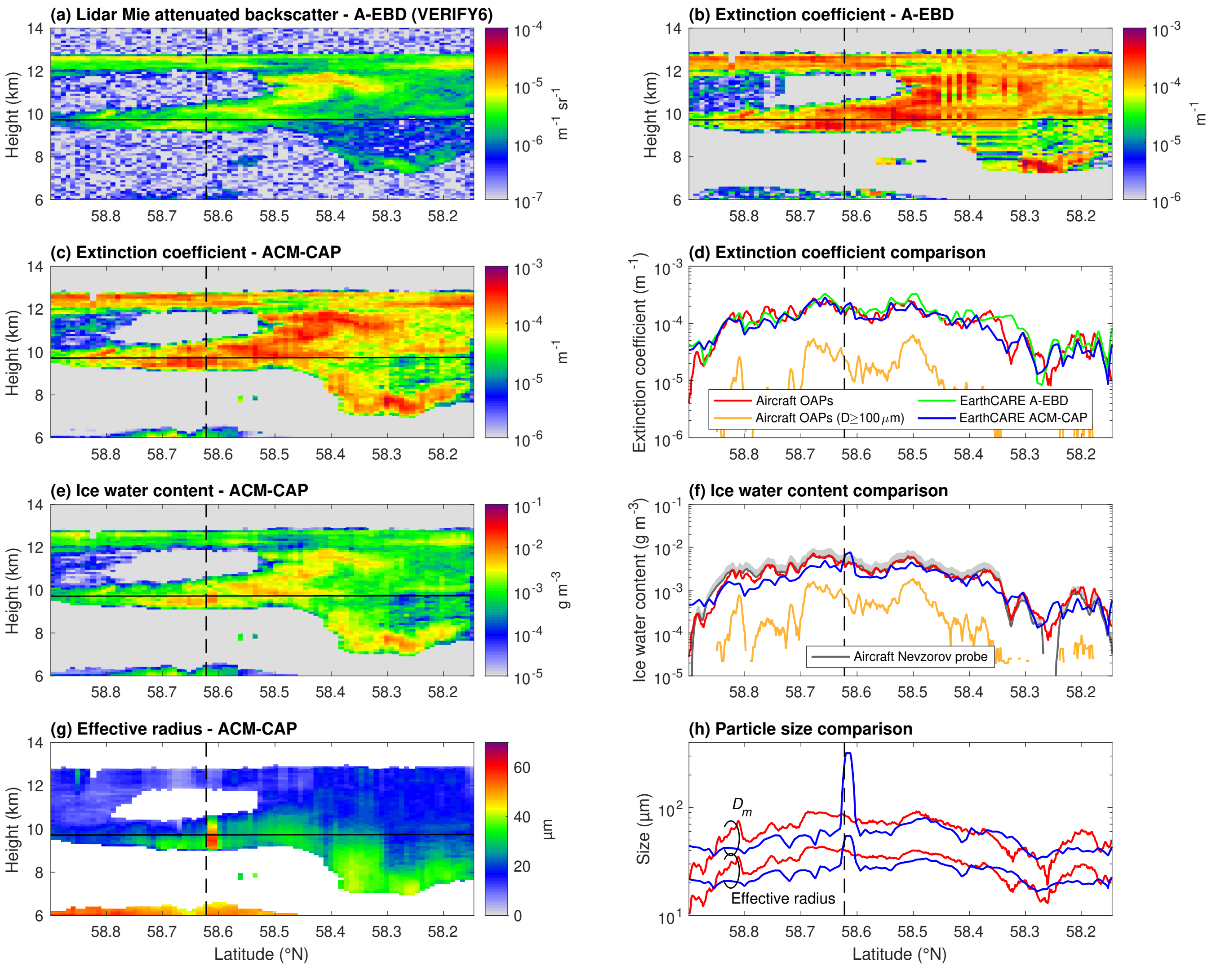


**Figure 2.** Lidar measurements and comparisons of retrievals for the VERIFY6 flight: (a) attenuated 355-nm backscatter measured by EarthCARE's lidar from the A-EBD product, (b) retrieved ice extinction coefficient from the lidar-only A-EBD product, (c) retrieved extinction from the synergy ACM-CAP product, (d) comparison of these two extinction retrievals with aircraft measurements, (e) retrieved ice water content from ACM-CAP, (f) comparison of this retrieval, and one by C-FMR, with two corresponding aircraft measurements by the optical array probes assuming the BF95 mass–size relationship and the Nevzorov probe, (g) retrieved effective radius from ACM-CAP, and (h) comparison of $r_e$ and $D_m$ between ACM-CAP retrievals and aircraft measurements.

https://doi.org/10.5194/egusphere-2026-5054
Preprint. Discussion started: 31 August 2026


poorer agreement between the Nevzorov- and OAP-inferred IWC in Fig. 4f. We cannot rule out an error in the radar calibration at the time of this underflight, although the available sea-surface calibration data does not suggest a problem at this time.

VERIFY4 sampled much larger particles ($D_m \simeq 2$ mm) and Fig. 9b shows a 5–15 dB difference between $Z_{94}$ and $Z_{\mathrm{Ray}}$, yet the aircraft-estimated $Z_{94}$ is in excellent agreement with the EarthCARE measurements. This gives support to the use of SSRGA for computing $Z_{94}$ well outside the Rayleigh scattering regime. Nonetheless, this is only one flight and it would be very valuable to evaluate it using flights sampling even larger snowflakes.

### 4.2 Doppler velocity, terminal fall speed and vertical wind

In VERIFY6, the radar reflectivity was lower than the $-20$ dBZ required to make reliable Doppler measurements, so we first consider VERIFY2 shown in Fig. 3. Aside from the contamination when the radar detected the aircraft, the Doppler velocity measured by EarthCARE in panels c and d shows fluctuations with a horizontal scale of around 20 km. It is not obvious from EarthCARE alone whether these are primarily due to vertical wind $w$, fluctuations in terminal fall speed $v_D$, or simply autocorrelated instrument noise. Releases of the C-CD product up to baseline BC assumed a significant fraction of these fluctuations to be due to variations in $v_D$, but the $v_D$ calculated from aircraft size distributions in panel f shows only very small-scale variations, likely due to sampling noise of the OAPs. Updating C-CD to use much longer windows (see section 3.1) leads to most of the observed fluctuations in $v_D$ to be attributed to fluctuations in $w$, and the agreement with aircraft measurements in panel h is excellent, confirming the detection of gravity waves. Good agreement is also found for ECALOT6 (Fig. 7h) in which waves of amplitude around 1 m s$^{-1}$ were present; the match is not perfect between every peak and trough, but it should be stressed that the period of these waves is short so only a small mismatch in sampling time is enough to reduce the agreement. Indeed, the Brunt-Väisäla frequency calculated from the meteorological analysis of the European Centre for Medium-Range Weather Forecasts (ECMWF) for the ECALOT6 underflight suggested a wave period of only 8 minutes. Nonetheless, these two cases give us confidence that EarthCARE can measure the amplitude and phase of gravity waves in cloud.

No gravity waves are detected in the remaining two cases: the aircraft measurements during ECALOT 3 (Fig. 5h) show intermittent turbulence at much too small a scale for EarthCARE to measure, and very little activity in VERIFY4 (Fig. 9h). In both of these cases, the radar continues to report features with a horizontal scale of around 10 km (Figs. 5g and 9g) and an amplitude of around 0.3 m s$^{-1}$, but it is most likely that these are simply measurement uncertainty and indeed this amplitude is similar to the predicted uncertainty of EarthCARE's Doppler measurements (e.g., Kollias et al., 2014). It is notable that this instrument noise has no vertical coherence beyond the radar's vertical pulse length of 500 m, whereas the genuine gravity waves detected in Fig. 7g have vertical coherence. Conceivably it could be possible to devise an algorithm to quantify the vertical coherence and thereby distinguish weak gravity waves from instrument noise.

Comparing now the reflectivity-weighted terminal fall speed $v_T$, we see from Table 2 that for VERIFY2, ECALOT3 and ECALOT6, the aircraft-calculated $v_T$ was on average around 15% larger than the EarthCARE value, and 30% larger for VERIFY4. Note that in these comparisons the EarthCARE average $v_T$ should be reliable since vertical wind is assumed to average to close to zero over the $\sim$100 km flight leg. Therefore the differences are likely to be due to errors in the calculation of $v_T$ from aircraft size distributions. In ECALOT6 and VERIFY4, $v_T$ was computed assuming a density factor of $f_\rho = 0.1$;

https://doi.org/10.5194/egusphere-2026-5054
Preprint. Discussion started: 31 August 2026


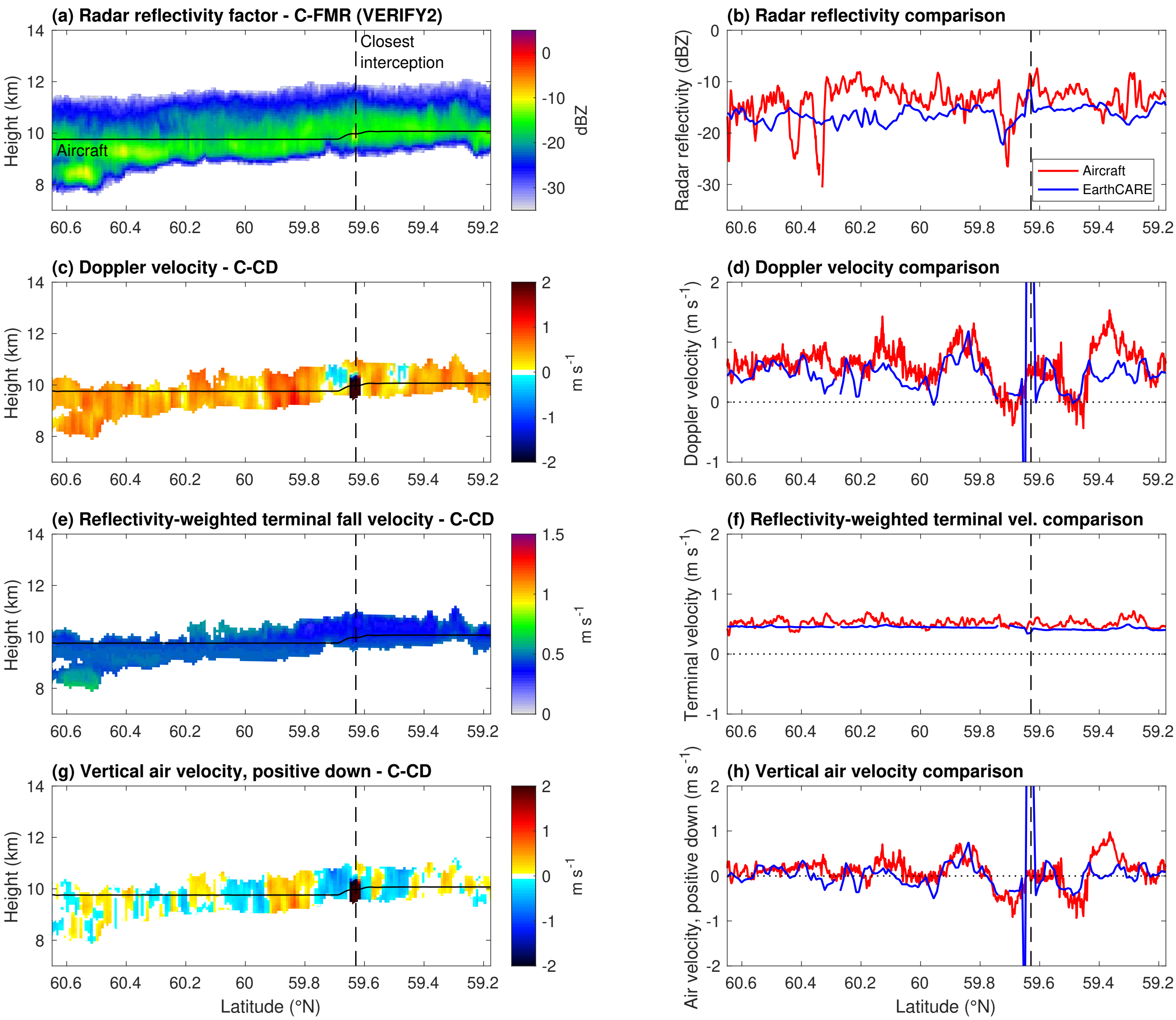


**Figure 3.** (a) EarthCARE radar reflectivity from the C-FMR product for frame 02531D on 7 November 2024, (b) comparison with reflectivity calculated from the ice PSD measured by FAAM during the VERIFY2 flight assuming the BF95 mass–size distribution, (c) EarthCARE Doppler velocity reported by C-CD and (d) corresponding comparison with the value from the aircraft combining the measured vertical air velocity and the estimated reflectivity-weighted terminal fall velocity from the PSD. The remaining panels display and compare the C-CD retrievals of terminal fall velocity and vertical air velocity. The aircraft is clearly seen in both EarthCARE's reflectivity and Doppler measurements. Aircraft measurements affected by air motion in panels d and h are shown at the raw 100-m resolution, while all other aircraft measurements are averaged along-track to 500 m. Note that all panels use the convention of positive indicating downward motion.

https://doi.org/10.5194/egusphere-2026-5054
Preprint. Discussion started: 31 August 2026


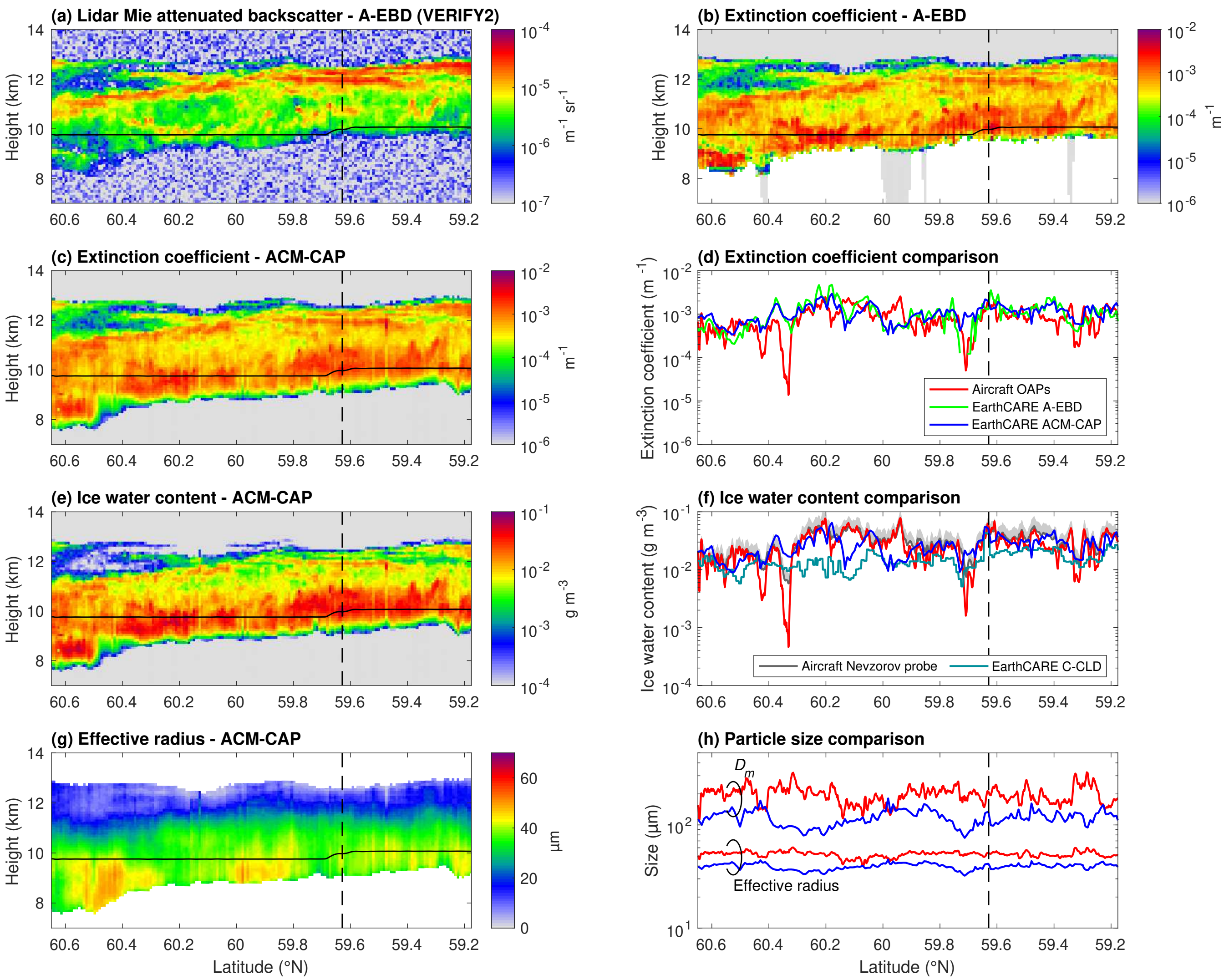


**Figure 4.** As Fig. 2 but for the VERIFY2 flight on 7 November 2024 (see also Fig. 3).

if this is reduced to 0 as used in the other cases, then the median $v_T$ values are reduced from 0.99 and 1.30 m s$^{-1}$ to 0.84 and 1.04 m s$^{-1}$ for the two cases, which brings them into much better agreement with EarthCARE. However, this leads to a much poorer match for $Z_{94}$, and IWC computed from the OAPs would not agree with the Nevzorov probe, and so it seems more likely to be to do with the Heymsfield and Westbrook (2010) fall speed model, possibly related to the appropriate cross-sectional area to use. It is beyond the scope of this paper to solve the issue, but until this is resolved it would be advisable not to use $v_T$ to attempt to retrieve $f_\rho$ in ACM-CAP, because its use of the Heymsfield-Westbrook model will tend to lead to $f_\rho$ being underestimated.

https://doi.org/10.5194/egusphere-2026-5054
Preprint. Discussion started: 31 August 2026


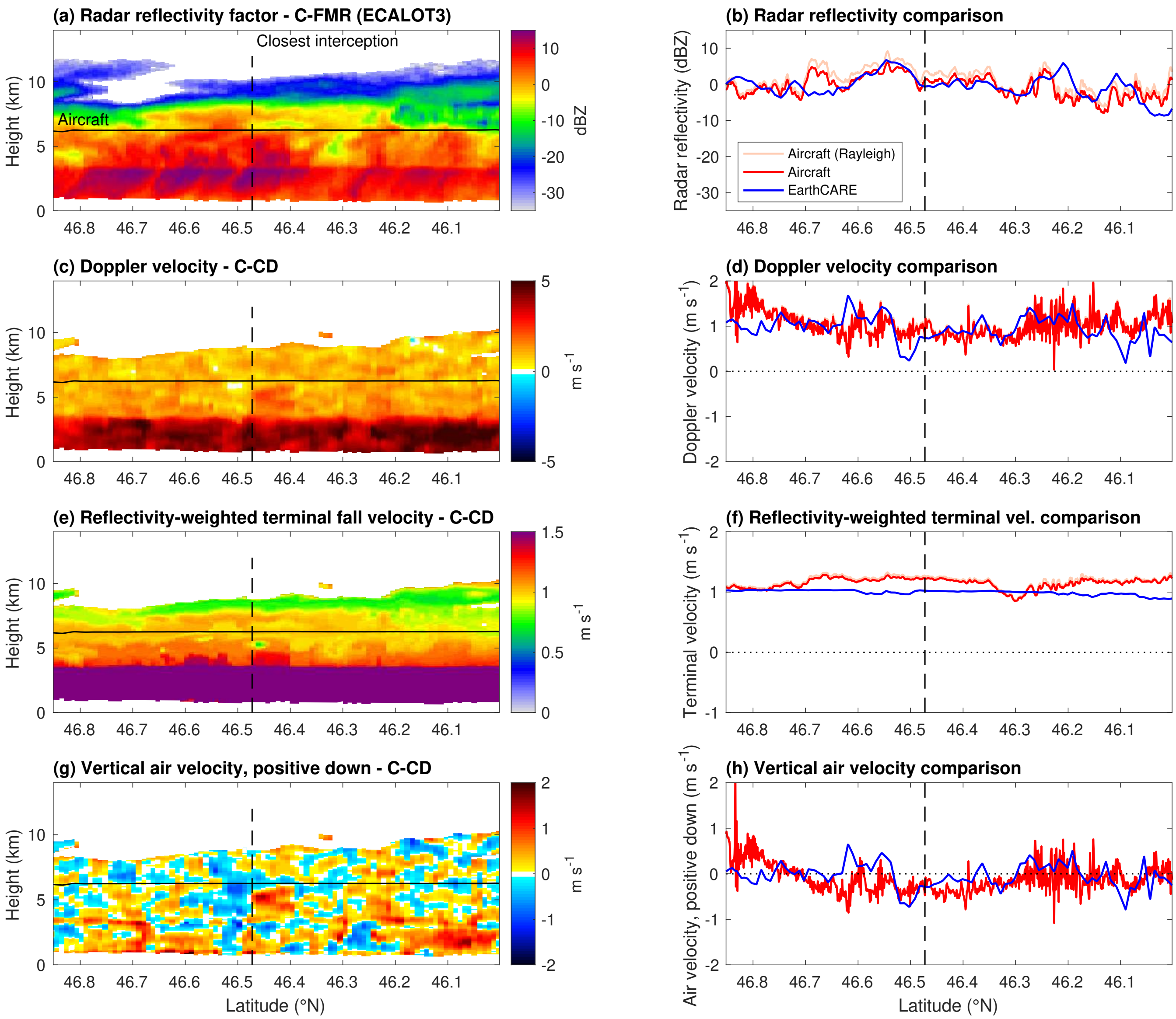


**Figure 5.** As Fig. 1 but for the ECALOT3 flight on 4 November 2024 corresponding to EarthCARE frame 02487D.

An intriguing finding in the VERIFY4 case in Fig. 10e is that 1 km above the aircraft at a temperature of around $-15$°C, $v_T$
300 retrieved from EarthCARE decreases by around 20 cm s$^{-1}$ as the ice falls, and this coincides with an increase in $Z_{94}$. C-CD uses the local correlation of $Z_{94}$ and $v_D$ to infer $v_T$, and here there is an anti-correlation. Ice deceleration at this temperature has also been reported from ground-based radars (von Terzi et al., 2022). Conceivably, rapid plate-like or dendritic growth could lead to horizontally oriented particles with a larger projected-area-to-mass ratio than the particles falling from above, leading to slower terminal fall speeds. The CIP-15 imagery for this case reveals the presence of irregular particles, mostly aggregates

https://doi.org/10.5194/egusphere-2026-5054
Preprint. Discussion started: 31 August 2026


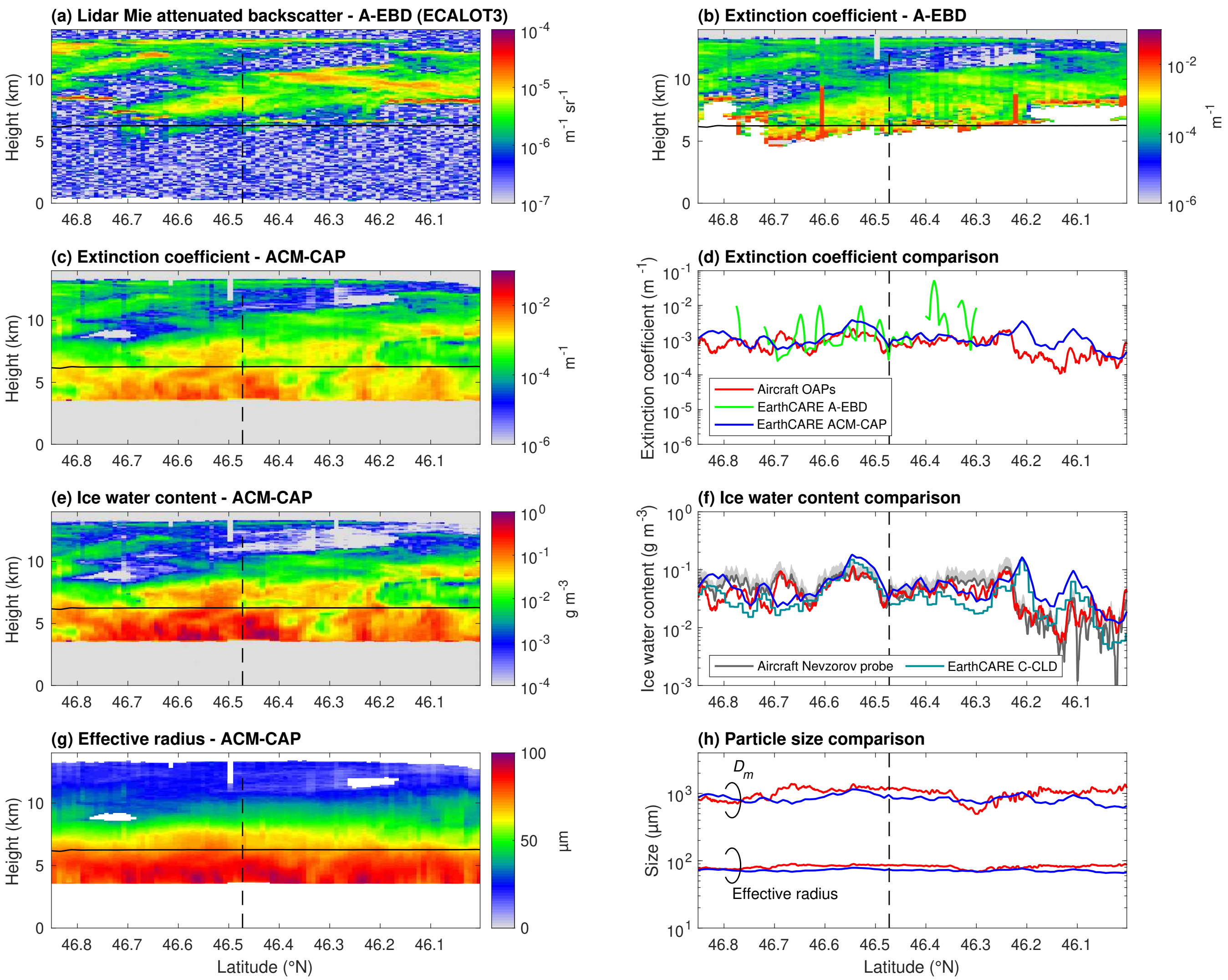


**Figure 6.** As Fig. 2 but for the ECALOT3 flight on 4 November 2024 (see also Fig. 1). Note that the A-EBD lidar-only extinction retrieval (panel b) includes the contribution from liquid water layers 8 km, but the ACM-CAP synergy extinction retrieval (panel c) shows only the contribution from ice cloud.

of plates, with the individual plate crystals within the aggregates being of typically 300–600 $\mu$m in size. Until we are able to properly explain and model this local anti-correlation between $Z_{94}$ and $v_T$, ACM-CAP will not rely strongly on $v_T$ in its ice retrieval.

https://doi.org/10.5194/egusphere-2026-5054
Preprint. Discussion started: 31 August 2026


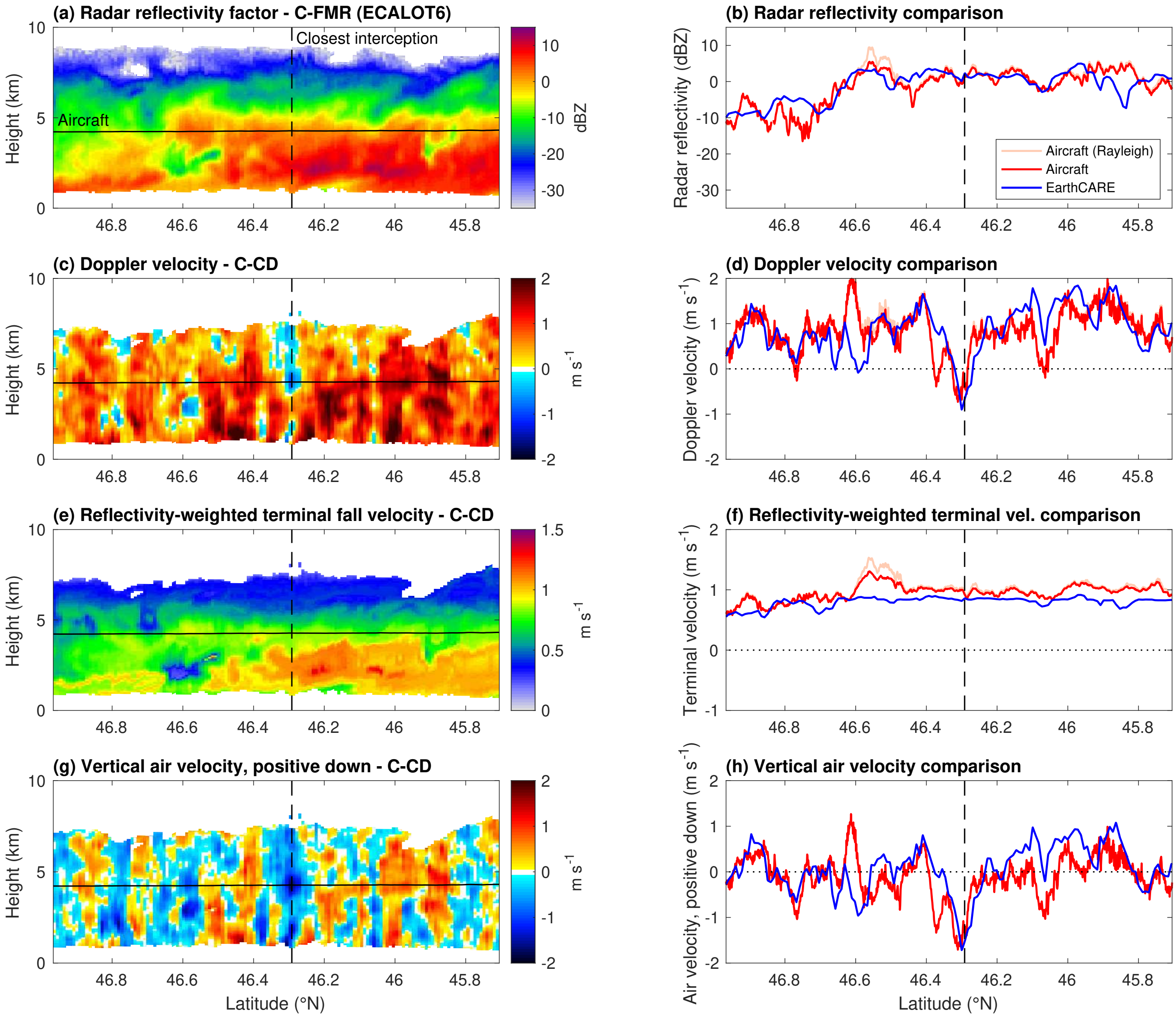


**Figure 7.** As Fig. 1 but for the ECALOT6 flight on 27 January 2025 corresponding to EarthCARE frame 03794D, where the OAPs have been processed using the mass–size relationship for denser ice particles ($f_\rho = 0.1$) described in the text.

https://doi.org/10.5194/egusphere-2026-5054
Preprint. Discussion started: 31 August 2026


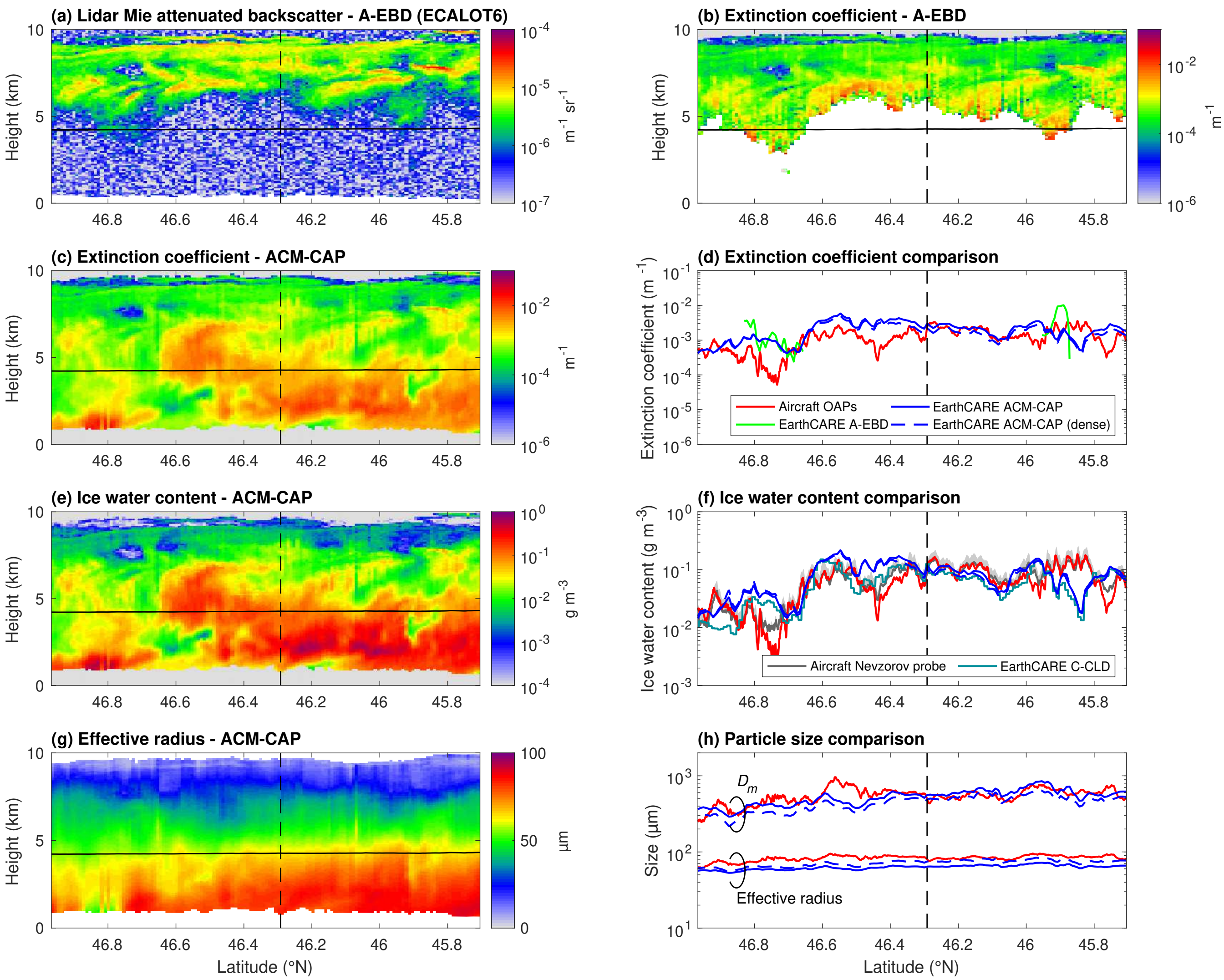


**Figure 8.** As Fig. 2 but for the ECALOT6 flight on 27 January 2025 (see also Fig. 7) and with the OAPs processed using the denser mass–size relationship described in the text.

### 4.3 C-CLD cloud and precipitation retrievals

C-CLD retrievals of ice water content (IWC), which rely on the radar reflectivity and terminal fall speed alone, show performance broadly comparable to the synergistic ACM-CAP retrievals in these cases. For a single-instrument algorithm, this level of agreement is encouraging. With the exception of VERIFY6 (where the Doppler measurements are not sufficiently reliable because of the low radar reflectivity, so no C-CLD retrieval is attempted) the retrieved values reproduce the overall magnitude and structure of IWC observed by the aircraft. Remaining differences are generally consistent with the expected sensitivity to retrieval assumptions and known instrument limitations.

https://doi.org/10.5194/egusphere-2026-5054
Preprint. Discussion started: 31 August 2026


### 4.4 A-EBD extinction retrievals

EarthCARE's lidar only penetrated the cloud consistently to the level of the aircraft in the two most optically thin cases, VERIFY6 and VERIFY2, where Figs. 2d and 4d show very good agreement in extinction coefficient, $\alpha$, between A-EBD retrievals and aircraft measurements. The modest differences in the median reported in Table 2 are within the uncertainty to be expected from the use of an empirical area-size relationship in (5). In ECALOT3, the aircraft was flying just at the level where the lidar was becoming fully attenuated, and in the latitude range 46.2–46.4° it appears that there could have been a layer of supercooled liquid cloud a short distance above the aircraft; these two factors explain the much noisier extinction retrieval in Fig. 6b. In the final two cases, the aircraft was almost entirely below the height at which the lidar signal became totally attenuated.

### 4.5 ACM-CAP microphysical retrievals

We last examine the performance of ACM-CAP's retrievals of $\alpha$, IWC and $r_e$, although since $r_e$ is related to the other two via (6), there are only two degrees of freedom to be assessed. In the first two cases, $\alpha$ was very tightly constrained by the lidar observations so ACM-CAP had a similar performance to A-EBD for this variable (Figs. 2d and 4d). Note that since ACM-CAP also makes use of the radar reflectivity, the spike in measured $Z_{94}$ when the radar detected the aircraft also fed through to a small blip in retrieved $\alpha$.

An interesting feature of the VERIFY2 flight occurred at 59.7°N when the aircraft, which was flying from north to south, passed out of the cloud base and the decision was taken at the time to gain altitude to remain within the cloud. The lidar retrievals in Fig. 4b correctly identified cloud base, and the drop in $\alpha$ at this point closely matches the aircraft measurements in Fig. 4d. However, due to the 500-m pulse length of the radar, the aircraft appeared to be entirely in cloud both in the $Z_{94}$ image in Fig. 3a and in the retrieved $\alpha$ using the synergy of radar and lidar in Fig. 4c. This highlights a potential vertical smearing effect in any retrieval that makes use of the radar, which adds an additional source of noise when comparing to aircraft in-situ measurements.

The remaining three cases involve progressively less information being available from the lidar due to attenuation, so providing an excellent test of the ability of ACM-CAP to blend smoothly from the radar-lidar region down to the radar-only region where it is more dependent on prior assumptions. In ECALOT3, the $\alpha$ retrieval in Fig. 6c is smooth across the point where the lidar loses signal, which occurs at around the altitude of the aircraft. Both $\alpha$ and IWC retrievals appear to agree well the aircraft measurements (Figs. 6d and 6f) but diverge south of a latitude of 46.25°N, i.e. beyond around 50 km from the point of closest interception. The two measures of particle size in Fig. 6h are both a little low compared to the aircraft measurements.

In ECALOT6 and VERIFY4 (Figs. 8 and 10) the lidar was for the most part completely extinguished at the height of the aircraft, so the retrieval was mainly dependent on the radar reflectivity and the solar radiances, noting that the latter are sensitive to the optical depth of the entire column. The greatest challenge for ACM-CAP in these two cases, however, is that they had denser particles than predicted by the BF95 mass–size relationship, but ACM-CAP continued to assume BF95. This led to a substantial overestimate in both $\alpha$ and IWC (blue solid lines in Figs. 8d, 8f, 10d and 10f), but which was halved (or better) by

https://doi.org/10.5194/egusphere-2026-5054
Preprint. Discussion started: 31 August 2026


repeating the retrieval but using the same higher density $f_\rho = 0.1$ assumption as used in processing the aircraft measurements (blue dashed lines). The effective radius errors were also halved. Note that the effect of density is larger for VERIFY4 than for ECALOT6 because the larger sizes present mean a greater divergence between the particle masses given by (2) and (3), i.e. between $f_\rho = 0$ and 0.1. It is interesting that C-CLD retrievals of IWC performed better than ACM-CAP for these two cases while it performed a little less well for the lower-density cases (VERIFY2 and ECALOT3). This highlights that it should be possible to improve the treatment of ice density in ACM-CAP, perhaps by better use of the Doppler measurements or refinement of the a-priori assumptions in nimbostratus making use of a wider range of aircraft data not necessarily simultaneous with EarthCARE.

## 5 Conclusions

In this paper we have exploited in-situ measurements from five coordinated underflights of the EarthCARE satellite in ice clouds to evaluate some of the EarthCARE microphysical and dynamical retrievals, as well as to test radar ice scattering models. We find excellent agreement between the inferred vertical wind from EarthCARE and the corresponding aircraft measurements, validating a key assumption in the C-CD algorithm that the small-scale motions in the measured Doppler velocity can be attributed to air motion, while the more slowly varying component is due to terminal fall speeds. This is important for downstream scientific applications of these two variables. For example, vertically coherent wave motions are frequently observed in EarthCARE Doppler measurements over orography, often correlated with variations in cloud optical depth. Now that we have established that these are gravity waves whose amplitude and phase matches in-situ observations, we can proceed with confidence to quantitative studies of the impact of vertical motion on cloud microphysical properties, at least in stratiform clouds. Furthermore, EarthCARE's retrieved terminal velocity is immensely valuable for evaluating the assumed fall-speeds in weather and climate models. However, we do find that the predicted reflectivity-weighted terminal fall-speeds from the aircraft size distributions are 15–30% higher than those retrieved from EarthCARE, suggesting the need for further work to verify the Heymsfield and Westbrook (2010) ice fall-speed model.

We found that in three of the five flights, the Brown and Francis (1995) mass–size relationship provided the best match between IWC measured by the Nevzorov probe and calculated from the optical-array probe, while in the other two cases a slightly denser mass–size relationship provided the best fit. In four of the five flights, the average radar reflectivities calculated using these mass–size relationships agreed with EarthCARE measurements to within 0.5 dB, with the flights spanning radar reflectivity values from −30 to +10 dBZ. In the flight with the highest reflectivity, the SSRGA ice scattering model of Hogan and Westbrook (2014) correctly treated the large 5–15 dB correction for non-Rayleigh scattering effects. This gives confidence in the use SSRGA (coupled to the BF95 mass–size relationship) for both retrievals and radar forward-models used in model evaluation and data assimilation. Indeed, ECMWF began assimilation of EarthCARE radar data into its operational forecasts on 10 June 2026, using SSRGA to model ice-particle scattering. Nonetheless, further underflights are recommended in heavier snowfall to really test the limits of SSRGA.

https://doi.org/10.5194/egusphere-2026-5054
Preprint. Discussion started: 31 August 2026


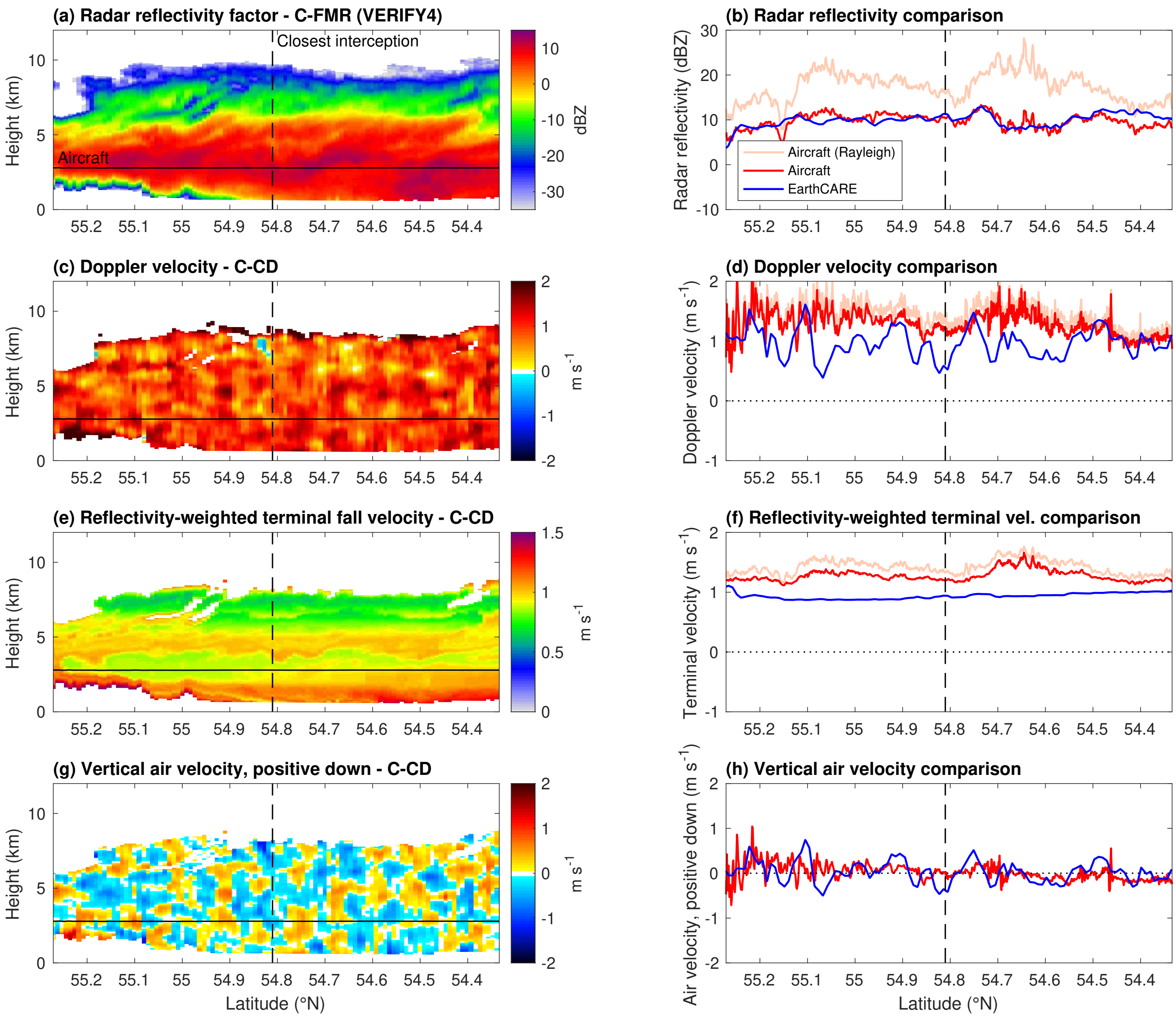


**Figure 9.** As Fig. 7 but for the VERIFY4 flight on 18 November 2024 corresponding to EarthCARE frame 02702D, and again using the mass–size relationship for denser ice particles described in the text. Also shown in panels (b), (d) and (f) are calculations from the aircraft size distributions of radar quantities that would be observed in the Rayleigh scattering regime, i.e. with a long-wavelength radar.

380 In terms of evaluating microphysical retrieval algorithms, the flights have provided very valuable information on the performance of the C-CLD, A-EBD and ACM-CAP algorithms. In terms of ice water content (IWC), C-CLD and ACM-CAP were within 33% of the aircraft in-situ measurements, except in the case of ACM-CAP for the two flights with denser ice particles than BF95. However, we found that if ACM-CAP assumed denser ice particles then the error reduced to less than 15%. This

https://doi.org/10.5194/egusphere-2026-5054
Preprint. Discussion started: 31 August 2026


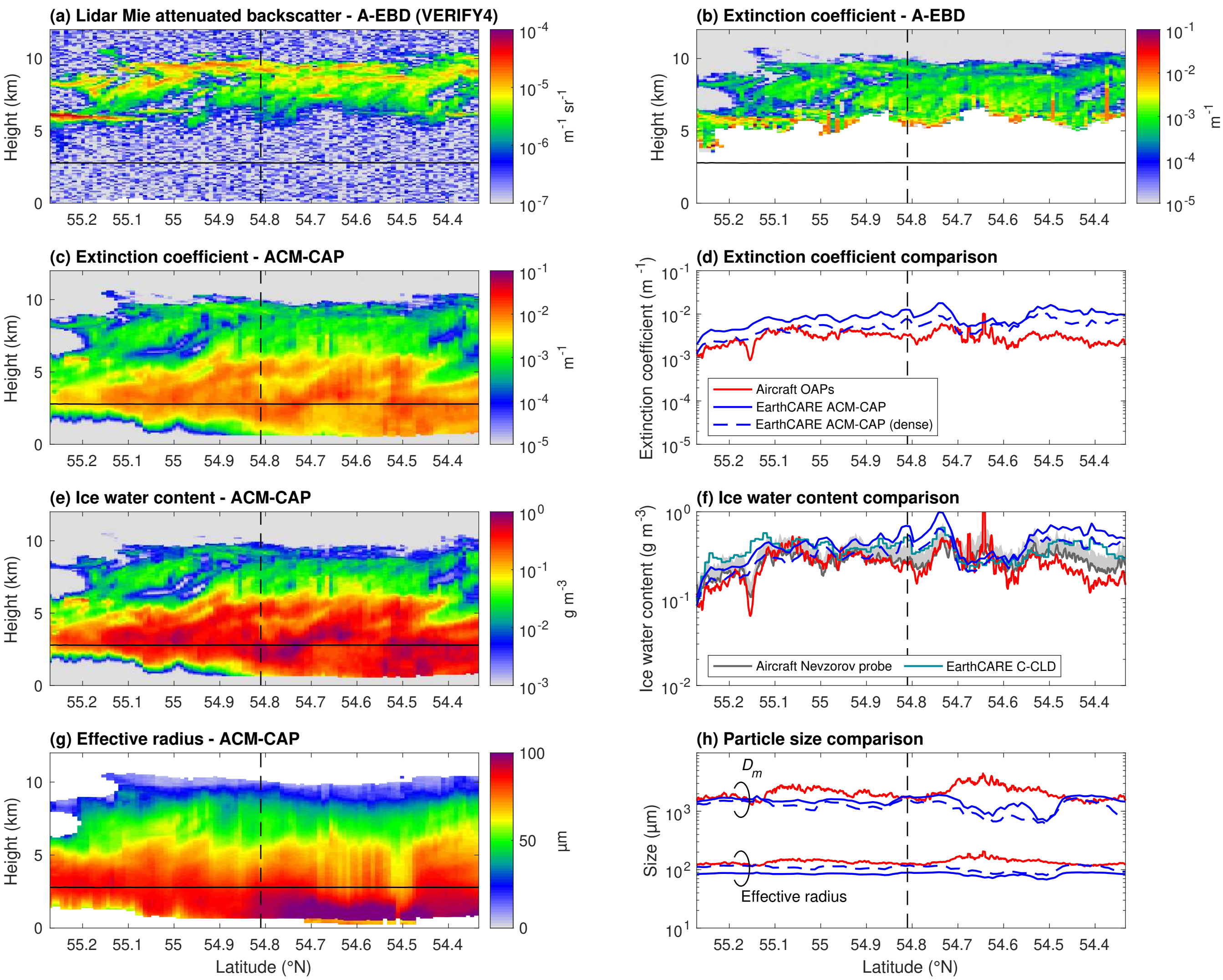


**Figure 10.** As Fig. 8 but for the VERIFY4 flight on 18 November 2024 (see also Fig. 9) and again using the denser mass–size relationship described in the text.

highlights the need to improve ACM-CAP's retrieval of density factor, via both a better temperature-dependent prior estimate, and better exploitation of the Doppler information. Currently ACM-CAP ingests the reflectivity-weighted terminal fall-speed, $v_T$, from C-CD but struggles to interpret it correctly in terms of density due to (1) the apparent overestimate of modelled $v_T$ identified in section 4.2, and (2) the difficulty in determining whether higher values of $v_T$ are due to denser particles or larger particles. In terms of retrieved extinction coefficient, the errors were generally a little larger than for IWC, and the retrieved effective radius from ACM-CAP was typically 15–25% too low.

https://doi.org/10.5194/egusphere-2026-5054
Preprint. Discussion started: 31 August 2026


All of these findings are being considered carefully in the ongoing development of these algorithms, but there is a need for further underflights in a wider range of conditions (both ice clouds and other types of cloud and precipitation) to further understand which aspects of the algorithms need improving, including the assumed shape of the size distribution, and the calculation of ice scattering properties used to forward-model the various instruments onboard EarthCARE.

*Data availability.* The colocated data from the aircraft and the various EarthCARE products for the five flights used in this paper are available in the dataset of Hogan et al. (2026).

*Author contributions.* RH performed the analysis of the data, produced the figures and led the writing of the paper. All authors contributed to discussions on interpreting the results, and provided suggestions on and contributions to the text. BPT, in discussion with KM and PK, produced and revised the C-CD and C-CLD products. SM produced and revised the ACM-CAP product. AK and ZQ produced the microphysical data from the Convair aircraft and assisted in its interpretation. KM provided assistance in interpreting data from the FAAM aircraft. DD produced and revised the A-EBD product.

*Competing interests.* PK is a member of the editorial board of Atmospheric Measurement Techniques. RH, DD and PK serve as editors for the special issue "Early Results from EarthCARE".

*Acknowledgements.* This research was supported by ESA's EarthCARE Data, Innovation and Science Cluster (ESA contract number 4000144997/24/I-NS). The VERIFY campaign was supported by ESA (contract number 4000146256/24/NL/JB) and the UK National Centre for Earth Observation. The ECALOT campaign was supported by Environment and Climate Change Canada, National Research Council Canada, and Canadian academic research institutes including McGill University, Université du Québec à Montréal and the University of Toronto. Funding for the FAAM Airborne Laboratory was discontinued at the end of March 2026, and we wish to thank the FAAM team for supporting a very wide range of important atmospheric research from this world-class platform over the past 25 years.

https://doi.org/10.5194/egusphere-2026-5054
Preprint. Discussion started: 31 August 2026


## References

Atlas, R. and Bretherton, C. S., 2023: Aircraft observations of gravity wave activity and turbulence in the tropical tropopause layer: prevalence, influence on cirrus clouds, and comparison with global storm-resolving models. *Atmos. Chem. Phys.,* **23,** 4009–4030. https://doi.org/10.5194/acp-23-4009-2023.

Brown, P. R. A., and P. N. Francis, 1995: Improved measurements of the ice water content in cirrus using a total-water probe. *J. Atmos. Oceanic Technol.,* **12,** 410–414. https://doi.org/10.1175/1520-0426(1995)012<0410:IMOTIW>2.0.CO;2.

Cotton, R. J., Field, P. R., Ulanowski, Z., Kaye, P. H., Hirst, E., Greenaway, R. S., Crawford, I., Crosier, J. and Dorsey, J., 2013: The effective density of small ice particles obtained from in situ aircraft observations of mid-latitude cirrus. *Q. J. R. Meteorol. Soc.,* **139,** 1923–1934. https://doi.org/10.1002/qj.2058.

Delanoë, J., and Hogan, R. J., 2008: A variational scheme for retrieving ice cloud properties from combined radar, lidar, and infrared radiometer, *J. Geophys. Res.,* **113,** D07204, https://doi.org/10.1029/2007JD009000.

Donovan, D. P., van Zadelhoff, G.-J., and Wang, P., 2024: The EarthCARE lidar cloud and aerosol profile processor (A-PRO): the A-AER, A-EBD, A-TC, and A-ICE products. *Atmos. Meas. Tech.,* **17,** 5301–5340. https://doi.org/10.5194/amt-17-5301-2024.

Field, P. R., Hogan, R. J., Brown, P. R. A., Illingworth, A. J., Choularton, T. W., and Cotton, R. J., 2005: Parametrization of ice-particle size distributions for mid-latitude stratiform cloud. *Q. J. R. Meteorol. Soc.,* **131,** 1997–2017. https://doi.org/10.1256/qj.04.134.

Fielding M. D., and Janisková, M., 2020: Direct 4D-Var assimilation of space-borne cloud radar reflectivity and lidar backscatter – 1. Observation operator and implementation. *Q. J. R. Meteorol. Soc.,* **146,** 3877–3899. https://doi.org/10.1002/qj.3878.

Francis, P. N., Hignett, P., and Macke, A., 1998: The retrieval of cirrus cloud properties from aircraft multi-spectral reflectance measurements during EUCREX'93. *Q. J. R. Meteorol. Soc.,* **124,** 1273–1291. https://doi.org/10.1002/qj.49712454812.

Heymsfield, A. J., and C. D. Westbrook, 2010: Advances in the estimation of ice particle fall speeds using laboratory and field measurements. *J. Atmos. Sci.,* **67,** 2469–2482, https://doi.org/10.1175/2010JAS3379.1.

Hogan, R. J., 2006: Fast, approximate calculation of multiply scattered lidar returns. *Applied Optics,* **45,** 5984-5992. https://doi.org/10.1364/AO.45.005984.

Hogan, R. J., and C. D. Westbrook, 2014: Equation for the microwave backscatter cross section of aggregate snowflakes using the Self-Similar Rayleigh–Gans Approximation. *J. Atmos. Sci.,* **71,** 3292–3301, https://doi.org/10.1175/JAS-D-13-0347.1.

Hogan, R. J., Field, P. R., Illingworth, A. J., Cotton, R. J. and Choularton, T. W., 2002: Properties of embedded convection in warm-frontal mixed-phase cloud from aircraft and polarimetric radar. *Q. J. R. Meteorol. Soc.,* **128,** 451–476. https://doi.org/10.1256/003590002321042054.

Hogan, R. J., M. P. Mittermaier, and A. J. Illingworth, 2006: The retrieval of ice water content from radar reflectivity factor and temperature and its use in evaluating a mesoscale model. *J. Appl. Meteor. Climatol.,* **45,** 301–317. https://doi.org/10.1175/JAM2340.1.

Hogan, R. J., L. Tian, P. R. A. Brown, C. D. Westbrook, A. J. Heymsfield, and J. D. Eastment, 2012: Radar scattering from ice aggregates using the horizontally aligned oblate spheroid approximation. *J. Appl. Meteor. Climatol.,* **51,** 655–671. https://doi.org/10.1175/JAMC-D-11-074.1.

Hogan, R. J., Honeyager, R., Tyynelä, J. and Kneifel, S., 2017: Calculating the millimetre-wave scattering phase function of snowflakes using the self-similar Rayleigh–Gans Approximation. *Q. J. R. Meteorol. Soc.,* **143,** 8340–844. https://doi.org/10.1002/qj.2968.

Hogan, R. J., Puigdomènech Treserras, B., Mason, S. L., Korolev, A., Qu, Z., Mroz, K., Donovan, D. P., Kollias, P., and Fielding, M. D., 2026: Colocated EarthCARE retrievals and aircraft in-situ measurements of ice clouds (Version 1.0) [Data set]. Zenodo. https://doi.org/10.5281/zenodo.22043988.

Illingworth, A. J., Barker, H. W., Beljaars, A., Ceccaldi, M., Chepfer, H., Clerbaux, N., Cole, J., Delanoë, J., Domenech, C., Donovan, D. P., Fukuda, S., Hirakata, M., Hogan, R. J., Huenerbein, A., Kollias, P., Kubota, T., Nakajima, T., Nakajima, T. Y., Nishizawa, T., Ohno, Y., Okamoto, H., Oki, R., Sato, K., Satoh, M., Shephard, M. W., Velázquez-Blázquez, A., Wandinger, U., Wehr, T., and van Zadelhoff, G.-J., 2015: The EarthCARE satellite: The next step forward in global measurements of clouds, aerosols, precipitation, and radiation. *B. Am. Meteorol. Soc.,* **96,** 1311–1332. https://doi.org/10.1175/BAMS-D-12-00227.1.

Irbah, A., Delanoë, J., van Zadelhoff, G.-J., Donovan, D. P., Kollias, P., Puigdoménech Treserras, B., Mason, S., Hogan, R. J., and Tatarevic, A., 2023: The classification of atmospheric hydrometeors and aerosols from the EarthCARE radar and lidar: the A-TC, C-TC and AC-TC products. *Atmos. Meas. Tech.,* **16,** 2795–2820, https://doi.org/10.5194/amt-16-2795-2023.

Jakob, C., 2002: Ice clouds in numerical weather prediction models – Progress, problems and prospects. In *Cirrus,* eds. D. Lynch et al., pp. 327–345, Oxford Univ. Press, New York.

Kollias, P., S. Tanelli, A. Battaglia, and A. Tatarevic, 2014: Evaluation of EarthCARE Cloud Profiling Radar Doppler velocity measurements in particle sedimentation regimes. *J. Atmos. Oceanic Technol.,* **31,** 366–386. https://doi.org/10.1175/JTECH-D-11-00202.1.

Kollias, P., Puidgoménech Treserras, B., Battaglia, A., Borque, P. C., and Tatarevic, A.: Processing reflectivity and Doppler velocity from EarthCARE's cloud-profiling radar: the C-FMR, C-CD and C-APC products. *Atmos. Meas. Tech.,* **16,** 1901–1914. https://doi.org/10.5194/amt-16-1901-2023.

Mason, S. L., Chiu, C. J., Hogan, R. J., Moisseev, D., and Kneifel, S., 2018: Retrievals of riming and snow density from vertically pointing Doppler radars. *J. Geophys. Res. Atmos.,* **123,** 13,807–13,834. https://doi.org/10.1029/2018JD028603

Mason, S. L., Hogan, R. J., Bozzo, A., and Pounder, N. L., 2023: A unified synergistic retrieval of clouds, aerosols, and precipitation from EarthCARE: the ACM-CAP product. *Atmos. Meas. Tech.,* **16,** 3459–3486. https://doi.org/10.5194/amt-16-3459-2023.

Mroz, K., Treserras, B. P., Battaglia, A., Kollias, P., Tatarevic, A., and Tridon, F., 2023: Cloud and precipitation microphysical retrievals from the EarthCARE Cloud Profiling Radar: the C-CLD product, 2023: *Atmos. Meas. Tech.,* **16,** 2865–2888. https://doi.org/10.5194/amt-16-2865-2023.

Puigdomènech Treserras, B., Kollias, P., Battaglia, A., Tanelli, S., and Nakatsuka, H., 2025: EarthCARE's cloud profiling radar antenna pointing correction using surface Doppler measurements. *Atmos. Meas. Tech.,* **18,** 5607–5618. https://doi.org/10.5194/amt-18-5607-2025.

Puigdomènech Treserras, B., Kollias, P. and Battaglia, A., 2026: Retrieval and climatology of hydrometeor sedimentation velocity from EarthCARE cloud profiling radar observations. *Manuscript in preparation*.

Protat, A., and Williams, C. R., 2011: The Accuracy of Radar Estimates of Ice Terminal Fall Speed from Vertically Pointing Doppler Radar Measurements. *J. Appl. Meteor. Climatol.,* **50,** 2120–2138. https://doi.org/10.1175/JAMC-D-10-05031.1.

Sasikumar, S., Battaglia, A., Puigdomènech Treserras, B., and Kollias, P., 2025: The Estimation of Path Integrated Attenuation for the EarthCARE Cloud Profiling Radar. *EGUsphere,* **2025,** 1–25. https://doi.org/10.5194/egusphere-2025-3573.

von Terzi, L., Dias Neto, J., Ori, D., Myagkov, A., and Kneifel, S., 2022: Ice microphysical processes in the dendritic growth layer: a statistical analysis combining multi-frequency and polarimetric Doppler cloud radar observations. *Atmos. Chem. Phys.,* **22,** 11795–11821. https://doi.org/10.5194/acp-22-11795-2022.

Williams, A., and D. Marcotte, 2000: Wind measurements on a maneuvering twin-engine turboprop aircraft accounting for flow distortion. *J. Atmos. Oceanic Technol.,* **17,** 795–810. https://doi.org/10.1175/1520-0426(2000)017<0795:WMOAMT>2.0.CO;2.